Green Chemistry

PAPER

View Article Online
View Journal | View Issue

Cite this: *Green Chem.*, 2025, **27**, 13893

A greener strategy for ultra-fast adsorption-promoted ozonation of livestock-excreted pharmaceuticals by co-pyrolysis of steel converter slag and biogas residues: synergistic effects, environmental impacts and DFT study

Muhammad Noman,[a,b] Dinkayehu Tsegaye Awugichew,[a,b] Guangwei Yu *[a] and Tekuma Abdisa Bakare[a,b]

China is the biggest pork-producing country, consequently raising serious environmental threats, due to the direct irrigation of untreated swine urine containing emerging toxic antibiotic residues like ofloxacin. Similarly, China's steel and biogas industries generate steel converter slag (SCS) residue (120 million tons annually) and biogas residue (BR). The disposal of SCS and BR is not eco-friendly due to the potential risk of leaching of heavy metals and eutrophication. Herein, the eco-friendly, one-pot co-pyrolysis of BR and SCS successfully achieved synergistic integration at various temperatures under an N_2 atmosphere, as confirmed by characterization studies. Adsorption-promoted ultra-fast ozonation over an Fe-SCS@BR-700 °C catalyst eliminated OFL (20 mg L^{-1}) and toxic organic pollutants of swine urine. High-Performance Liquid Chromatography (HPLC) and Triple Quadrupole Liquid Chromatography-Mass Spectrometry (QTRAP ABI-3200) were employed successfully to trace and remove (<0.01 ppm) more than 16 toxic pharmaceuticals. ICP-MS and toxicity assessment revealed 0.2 g as a safer dosage. Wheat grains and *Escherichia coli* growth were seen in ozonated urine. Density functional theory and electron paramagnetic resonance revealed abundant active sites, exponential electron transfer, and ROS generation like hydroxyl radicals (•OH), superoxide ($O_2^{\bullet-}$), and singlet oxygen ($^1O_2$) *via* ozone decomposition. Magnetization without regeneration enables robust recovery and recyclability. Comparatively, Fe-SCS@BR-700 °C reduces emissions, resource use, and costs more effectively. This study successfully established a greener, economical, and efficient heterogeneous catalyst to eliminate toxic pollutants from real swine urine at a small pigsty for safer urine resource irrigation, showing a sustainable approach for treating waste by waste.

Received 2nd August 2025,
Accepted 16th September 2025

DOI: 10.1039/d5gc04029a

rsc.li/greenchem

Green foundation

1. This study explores green and efficient waste reuse by converting hazardous steel converter slag (120 million tons per year in China) and biogas residues into a functional nano-composite, preventing landfill and heavy metal leaching, and offering a low-cost green, recyclable, and stable alternative.
2. One-pot co-pyrolysis of renewable feedstocks like carbon-rich biogas residues (waste prevention) with steel converter slag (atom-economy) was performed at an energy-efficient temperature (700 °C) under an N_2 atmosphere, avoiding toxic solvents. This novel catalyst successfully eliminated the toxic pharmaceuticals in swine urine by synergistically enhancing ozonation *via* adsorption without toxic outputs, as an economical option for small pig farm urine treatment, confirmed by life cycle assessment.
3. Future directions may involve exploring the real potential of industrial and agricultural hazardous wastes for low-cost, green catalysts for environmental implications, life cycle analysis, and policy advocacy.

1. Introduction

China is the world's leading pork producer, accounting for nearly 50% of global intensive pig farming, through which 30% of antibiotics such as ofloxacin (OFL) are utilized, causing environmental threats due to mass irrigation of untreated pig excrement (5.4 kg of urine per pig per day).[1,2] By

[a]*State Key Laboratory of Advanced Environmental Technology, Institute of Urban Environment, Chinese Academy of Sciences, Xiamen, Fujian 361021, China. E-mail: gwyu@iue.ac.cn*
[b]*University of Chinese Academy of Sciences, Beijing 100049, China*

2030, antibiotic use could reach 107 472 tons per year.[3] Globally, developing regions traditionally use untreated pig urine mixed with manure for irrigation and as fertilizer, posing risks to human health and ecosystems, and facilitating the spread of antibiotic resistance genes (ARGs). Unfortunately, pig farms in Jizhou district, Hebei province, have been identified as the primary contributors to antibiotic pollution in local water reservoirs, leading to a heightened risk to children's health, indicating an urgent need for enhanced pig urine wastewater treatment and regulatory measures.[4] Ofloxacin (OFL) is a commonly used antibiotic with broad-spectrum antibacterial properties. It enters the environment through urine, posing risks to drug-resistant bacteria, disrupting biological metabolism, especially in aquatic environments. OFL was the most commonly detected antibiotic in Jiaozhou Bay on the eastern coast of China.[5] Furthermore, due to the presence in Hebei province of 70% of China's small pigsties, OFL was also detected near rivers at 31.7 μg L^{-1}. OFL removal technologies like chlorination,[6] coagulation,[7] and electrochemical methods[8] involve highly complex, slow, and energy-intensive processes.[9] Notably, OFL behavior in the urine environment remains unexplored. Practical processing of real swine urine using biological,[10] anaerobic digester,[11] and membrane treatment[12] methods is often slow, ineffective, and costly. Photocatalytic degradation[13] and electrochemical techniques,[11] meanwhile, are light-dependent and energy-intensive, making them especially unsuitable for small pigsties. To date, the implications of high cost and low efficiency of real swine urine treatment methods have been observed by pig farmers. Overall, small farms lack basic infrastructure or rely on costly, outdated, and low-efficiency systems.[14] Hence, low-cost and eco-friendly technologies are urgently needed for safer swine urine resource utilization at small pigsties.

Due to rapid industrial development, the biogas and steel industries generate huge volumes of hazardous solid waste like steel converter slag (SCS) and biogas residue (BR). China, which is globally the largest steel producer, recycles only 35% of its SCS out of 120 million tons generated annually; the remainder is dumped into the open environment.[15] BR, utilized as fertilizer or landfill material, emits a foul odor and may contain pathogenic microorganisms and pollutants such as polychlorinated biphenyls and chlorinated paraffins. Both forms of waste can leach heavy metals into soil and water.[16,17] Furthermore, in the context of limited global waste management systems, the World Bank has estimated that global waste generation could surpass 3.40 billion tons by 2050.[18] Therefore, novel, greener, and advanced approaches, such as converting BR and SCS into green nanocomposites for practical environmental remediation, are crucial.

To address these hazardous waste products and associated environmental concerns, traditional catalyst synthesis, which is often complex and costly, is gradually shifting towards low-cost, non-toxic alternatives. Various agricultural, industrial, and municipal waste products are being repurposed as feedstocks for waste-derived catalysts through innovative scientific methods.[19] Current strategies and efforts to recover useful substances from industrial slag, such as alkali dissolution, acid precipitation, washing, and recrystallization,[20] are costly, water-intensive, and yield low outputs, while also causing secondary pollution, thus affecting sustainability and efficiency. Interestingly, advanced oxidation processes (AOPs), such as persulfate (PS) activation,[21] photocatalysis,[22] and Fenton-like oxidation,[23] have employed solid waste-derived carbonaceous catalysts (SW-CCs) for various environmental remediation applications. These systems rely on reactive oxygen species (ROS) including hydroxyl radicals ($^{\bullet}OH$), oxygen radicals ($O_2^{\bullet-}$), and singlet oxygen ($^1O_2$).[24] However, metal and non-metal synergy in such catalysts has yet to be elucidated. Given the coexistence of organic substances in BR and metals like Fe in SCS, there is an attractive prospect for *in situ* upcycling of hazardous industrial residues into efficient nano-composites for utilization in AOPs. This approach could pioneer the development of exogenous-free nano-composites derived from dual industrial residue streams, leveraging intrinsic organic and metallic constituents as precursors. Fortunately, an eco-friendly and low-cost, one-pot co-pyrolysis of SCS (Fe-rich) and BR (a carbon source) offers an innovative route for ozone (O_3) activation combined with adsorption, thereby enhancing ROS generation to degrade organic pollutants in real swine urine. SCS not only contributes increased active sites, improved graphitization, enhanced reusability, and greater conductivity of BR, but also provides Fe_2O_3, Fe_3O_4, and FeO (Fe^{2+}, Fe^{3+}, and Fe^0) to function as both an adsorbent and ion exchanger.[25,26] Thus, this strategy significantly enhances the utilization of all components of residues with potential synergistic effects, and can be expected to achieve sustainable utilization of low-cost industrial residues. Nevertheless, to the best of our knowledge, this is the first report of developing a green strategy employing an Fe-SCS@BR catalyst for adsorption-assisted, ultra-efficient catalytic ozonation to degrade various toxic antibiotics in real swine urine, supporting the novel concept of "treating waste with waste".

Herein, we propose, for the first time, a heterogeneous catalyst (Fe-SCS@BR), synthesized from industrial waste residues as raw materials, for the elimination of combined antibiotics, including OFL, from manure-separated swine urine under simulated urine conditions. This was achieved using a fixed-bed adsorption-promoted ozonation reactor operated under environmentally realistic conditions. Notably, enhanced degradation of various toxic emerging antibiotics, such as sulfamethoxazole, sulfamethazine, sulfamonomethoxine, quinolone antibiotics (fleroxacin, ofloxacin, norfloxacin), and antiparasitic drugs (*e.g.* levamisole), was observed in real swine urine. Characterization studies proved enhanced dispersion of Fe-ions, electron transfer ability, abundance of active sites, and catalyst reusability. The Fe-SCS@BR-700 °C catalyst exhibited optimum ROS generation for effective degradation, COD, and TOC removal of OFL and other toxic pharmaceuticals in real swine urine. Density functional theory (DFT) confirmed indirect O_3 adsorption and ROS affinity. Mechanistic studies and ICP-MS toxicity assays revealed a major role of $O_2^{\bullet-}$ alongside successful wheat and *E. coli* growth. This study contributes to novel and cost-effective implications for a greener environment.

2. Materials and methods

2.1 Materials and chemicals

All related information can be found in Section S1 of the SI.

2.2 Sampling and solution preparation

Raw BR was collected from the Xiamen Eastern Solid Waste Treatment Center, which was generated by livestock manure, while raw SCS was collected from the Anhui province steel industry. The chemical composition and properties of SCS and BR are shown in Table S1. Additionally, by utilizing the urine-manure separation method, real swine urine was collected from the treatment system (500 m^3 d^{-1}). Swine urine samples were collected in October (for the initial experiments) and December (for AOP experiments) 2024, from the Xinxing County pig farm, Yunfu City, Guangdong Province, China. For a lab-scale pilot study, fresh swine urine (5 L) samples were collected in acid-washed polyethylene bottles from a facility located on-site, involving primary clarifier, anaerobic fermentation, secondary clarifier, sedimentation, and chlorination disinfection processes. Notably, this system does not significantly degrade the organic matter and antibiotics contained in swine urine. Additionally, at the lab scale, by following standards, sample solutions of simulated urine and super deionized (SDI) water were also prepared containing ofloxacin (OFL) (20 mg L^{-1}). The characteristics of all solutions are mentioned in Section S2 and Fig. S8 of the SI.

2.3 Synthesis of the Fe-SCS@BR catalyst

As a pretreatment process, 5 g of raw SCS was rubbed and shaken three times alternately in super deionized water (SDI) (1000 mL) for 24 h and then washed with ethanol to remove dust and impurities. Afterward, the cleaned raw SCS was placed in an oven at 105 °C until it was dry. Then, 25 g of dried raw SCS was ground into fine 100 mesh powder by ball milling. Ecological one-step, co-pyrolysis of uniformly mixed BR and SCS in a ratio of 5 : 1 was then respectively conducted at 300 °C, 500 °C, and 700 °C for 45 min under an N_2 atmosphere (Table S1 and Fig. S7). Finally, all prepared catalysts were finely ground separately and labeled as Fe-SCS@BR-300 °C, Fe-SCS@BR-500 °C, and Fe-SCS@BR-700 °C, or SCS@BR-300-700°C as illustrated in Fig. 1(a).

2.4 Catalytic characterization

The physiological morphology and elemental composition of all catalysts were examined using advanced technologies, including energy dispersive spectroscopy (EDS), scanning electron microscopy (SEM), transmission electron microscopy (TEM), vibratory sample magnetometry (VSM), and X-ray photoelectron spectroscopy (XPS). All information related to catalytic characterization can be found in Section S3 of the SI.

2.5 Experimental procedure for adsorption-promoted catalytic ozonation degradation

All experiments were conducted in a 250 mL beaker at 25 °C ± 0.5 °C. Using standard procedures, simulated urine containing OFL (20 mg L^{-1}) was prepared from low-concentration ammonium bicarbonate (NH_4HCO_3) (0.20 mole per L)[27] (Section S2 and Fig. S8). An SDI solution of OFL was also prepared with similar concentration for comparison. Finally, the simulated urine and SDI solutions were stored at 4 °C in a refrigerator. Each 200 mL of solution contained 0.20 g (1 : 1000) of catalyst with continuous adsorption achieved using a magnetic stirrer (650 rpm), and O_3 flow of 5.50 ± 0.5 mg L^{-1} at 25 °C ± 0.5 °C, while the initial alkalinity was kept unchanged at pH 9.17 to resemble real conditions. Samples were collected at specific times and filtered into a conical centrifuge tube of 1.5 mL volume using a 0.45 μm polyether sulfone syringe, separately.

2.6 An adsorption-promoted lab-scale fixed-bed reactor for swine urine treatment – a pilot study

A lab-scale pilot study was adopted to reveal the potential of the optimum catalyst SCS@BR-700 °C for its actual environmental impact. First, fresh swine urine was pre-treated by vacuum filtration and filled into a liquid phase vial, whereupon solid phase extraction was performed to remove suspended solids. Second, nitrogen blowing was performed to remove volatile organic compounds. Swine urine samples were diluted using methanol, and a standard method for sample preparation was utilized. Finally, adsorption-supported catalytic ozonation degradation experiments were performed in a fixed-bed reactor (5 L) (Fig. S7b and Fig. 3h). All samples were collected and filtered at certain times. To detect the signal intensities of toxic pharmaceuticals in swine urine before and after reaction, QTRAP ABI-3200 mass spectrometry was employed. Further procedure details are mentioned in Section S4.

2.7 Analytical methods

OFL concentrations after the reaction were determined using an HPLC system (Agilent 1200) equipped with a C18 column (50 mm × 4.6 mm × 5 μm). Furthermore, UV-vis spectrophotometry was also employed to measure the OFL concentration at specified absorption wavelengths (nm). Triple Quadrupole Liquid Chromatography-Mass Spectrometry (QTRAP ABI-3200) was employed for detecting the signal intensities of toxic pharmaceuticals in real swine urine, while HPLC (Agilent 1200) was employed after catalytic ozonation of swine urine to measure the concentrations (mg L^{-1}) of degraded pharmaceuticals. Total organic carbon (TOC) and chemical oxygen demand (COD) were used for the measurement of biodegradable and non-biodegradable organic compounds. Suspended solids in the real swine urine were determined by the gravimetric method, while ammonia nitrogen (NH_3-N) contents were measured by the nano-reagent spectrophotometric method. Three-dimensional excitation–emission matrix fluorescence spectroscopy (3D-EEM) was used to measure organic decomposition after the reaction. Furthermore, all details of the measurement methods are provided in Section S5.

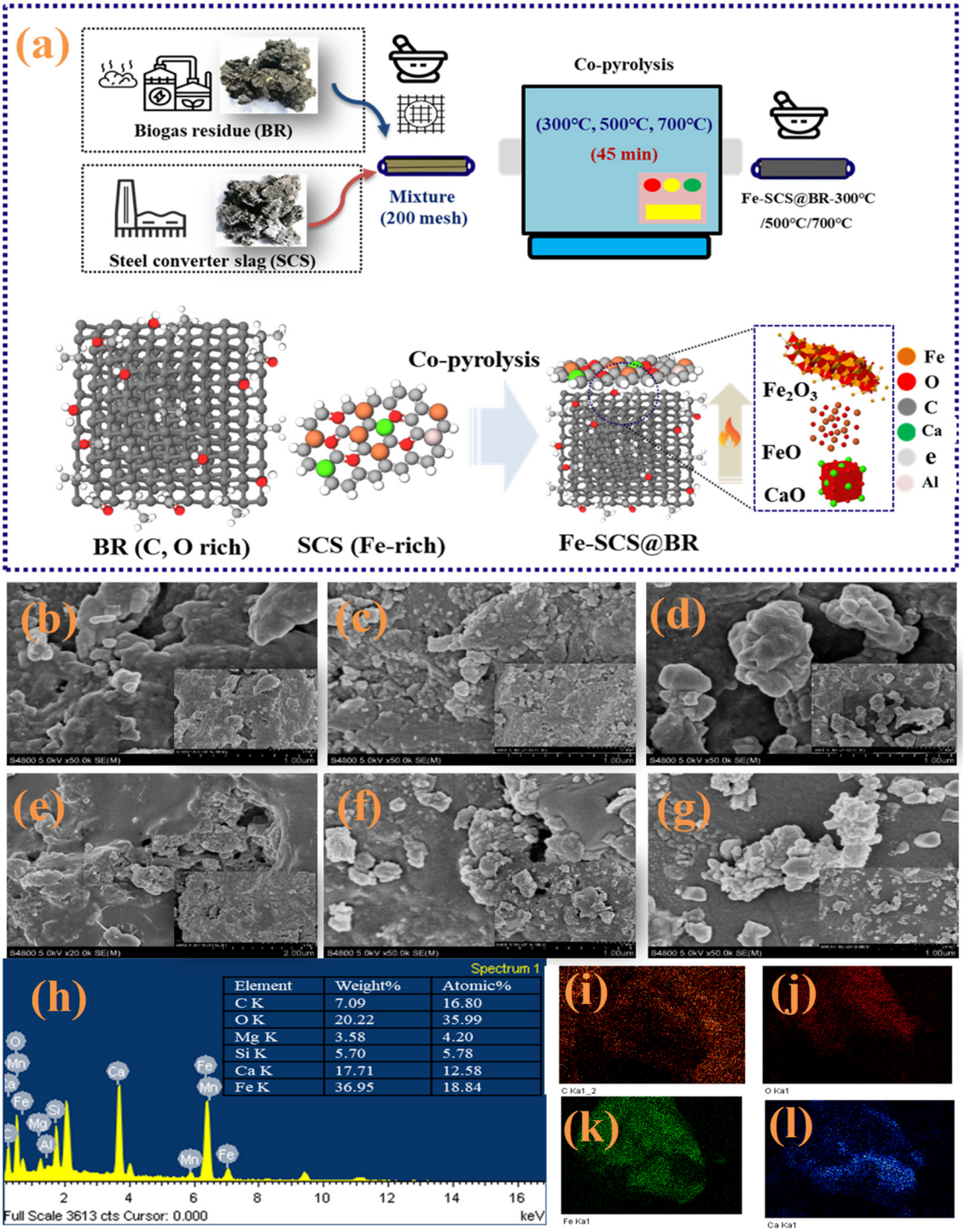

Fig. 1 (a) Schematic synthesis, (b) BR (biogas residue), (c) steel converter slag (SCS), (d) raw mixture (SCS : BR) (1 : 5), (e) Fe-SCS@BR-300 °C, (f) Fe-SCS@BR-500 °C, (g) Fe-SCS@BR-700 °C, (h) EDS of Fe-SCS@BR-700 °C, (i) C g, (j) O g, (k) Fe g and (l) Ca g.

3. Results and discussion

3.1 Characterization

Fig. 1(b–g) depicts the SEM images of raw BR, raw SCS, and their pre-pyrolyzed mixture, and pyrolyzed catalyst (Fe-SCS@BR) samples at different temperatures. Raw BR and SCS (Fig. 1b and c) can be easily distinguished before and after co-pyrolysis. Comparatively, SCS (Fig. 1c) shows irregular, compacted, and crystalline smooth surfaces. Fig. 1d shows the mixture (SCS : BR) before pyrolysis, with the irregular, rough, and grainy metal of SCS around the BR particles. Fig. 1(e–g) shows the Fe-SCS@BR samples pyrolyzed at various tempera-

tures, revealing the loose and porous surface of fused BR surrounded by SCS. Notably, at 300 °C to 700 °C, the loose, non-compacted, and bright surfaces were more visible.

The EDS mapping of Fe-SCS@BR-700 °C (Fig. 1h–l) confirms the significant contents of C, O, Ca, Al, Si, and Fe, due to their successful dispersion during co-pyrolysis. The images confirm that the uniform distribution of the metal content in SCS could enhance ozone decomposition. Hence, the higher temperature pyrolysis can enhance the metal active sites and facilitate superior synergy (Fig. S7a). Fig. 2a shows the XRD results of all raw and pyrolyzed catalysts. It was seen that the peaks for Fe_2O_3 (32–36°) and magnetite, Fe_3O_4, (44.86°) were shifted after pyrolysis, and the crystalline peaks for Fe_2O_3 (hematite) (2θ = 37.97°, 29.71°), Fe^0 (43.27°–48.74°), SiO_2 (2θ = 50.11°, 39.54°, 26.65), calcite (28.15°–32.02°), $CaCO_3$ (2θ = 36.54°, 29.30°), and quartz III (39.52°) were also successfully revealed. Notably, the distinct peaks for Fe^0 were seen at higher temperatures in favor of O_3 activation for ROS[28] (eqn (1) and (2)):

$$2Fe_2O_3 + 3C \rightarrow 4Fe^0 + 3CO_2, \quad (1)$$

$$Fe_2O_4 + 2C \rightarrow 2Fe^0 + 2CO_2. \quad (2)$$

Fig. 2b shows FT-IR spectra indicating all of the crucial functional groups in Fe-SCS@BR. Overall, signals for Si–O stretching, $CaCO_3$, and Fe–O vibrations were observed at 1036.59 cm^{-1}, 872.18 cm^{-1}, and 563.13 cm^{-1}, respectively.[29] The spectra for pristine and the raw mixture of SCS and BR reveal C–C stretching (1512.46 cm^{-1}), while after co-pyrolysis, C=C stretching (1645.05 cm^{-1}) was more obvious comparatively. The disappearance of OH peaks (2929.9–2803.14 cm^{-1}) occurred due to temperature increase, while those of the Fe–O bond became more apparent. Fig. 2c and Table S1 depict the results of the XPS analysis of non-pyrolyzed and pyrolyzed cata-

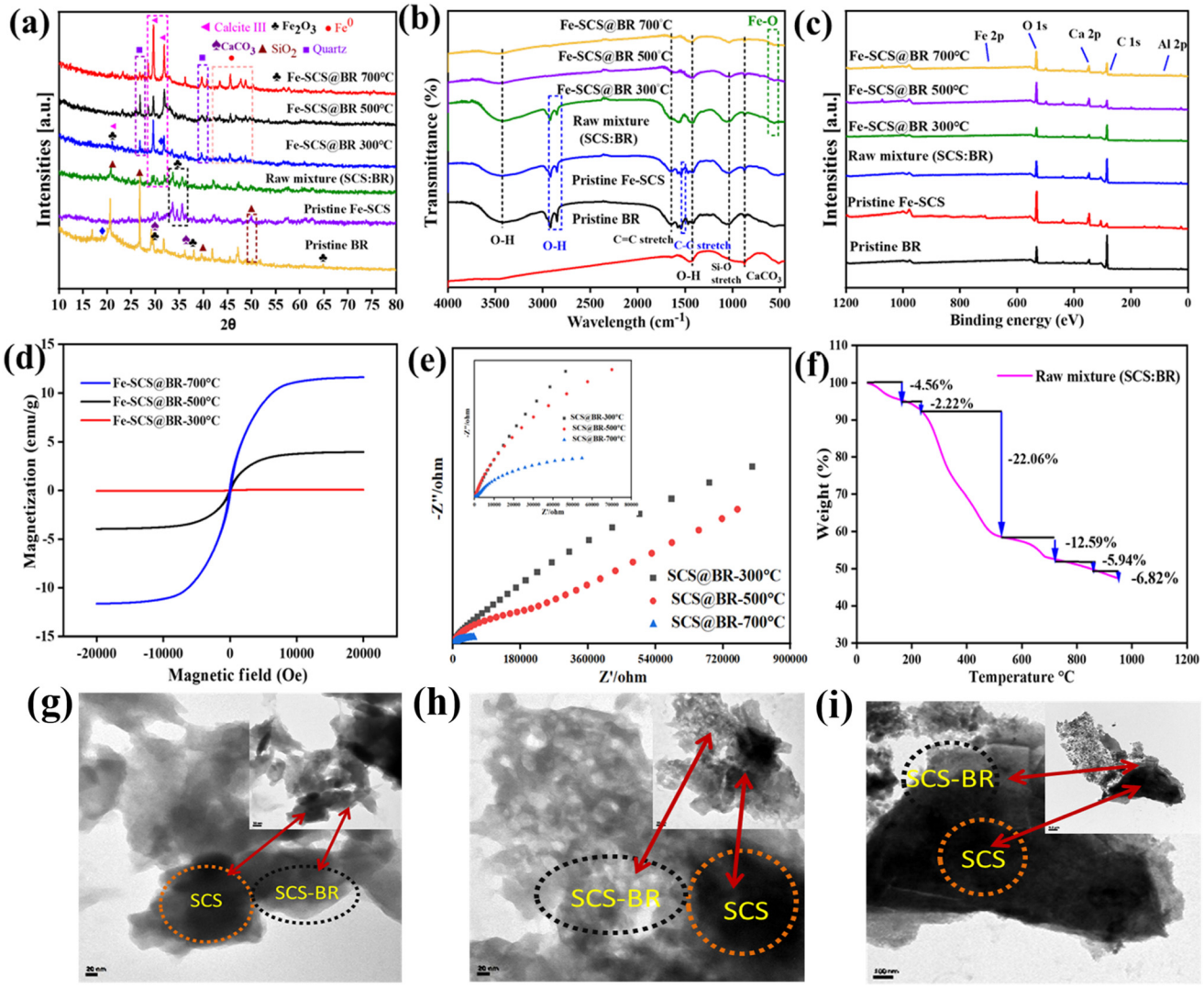

Fig. 2 (a) XRD, (b) FT-IR, (c) XPS of the BR, SCS and raw mixture (SCS : BR, Fe-SCS@BR (pyrolyzed)), (d) VSM, (e) EIS, (f) TGA of the mixture (SCS : BR) (1 : 5), and TEM of (g) Fe-SCS@BR-300, (h) Fe-SCS@BR-500 and (i) Fe-SCS@BR-700 °C.

lysts used to explore the elemental composition. Raw materials like BR and SCS have distinct C-1s, Ca-2p, and O-1s peaks, while the raw mixture revealed combined peaks. Interestingly, after co-pyrolysis at 300 °C, 500 °C, and 700 °C, the presence of Fe and Al increased from 0.04% to 0.016% and from 0.18% to 2.57%, respectively, while C, O, Ca, and Si showed some decline. Overall, the XPS results were consistent with the results of XRD, FT-IR, and SEM.

To reveal the separation and reusability of the catalyst, VSM of Fe-SCS@BR (300 °C, 500 °C, and 700 °C) samples was performed (Fig. 2d). Hysteresis loops of Fe-SCS@BR-300 °C/500 °C/700 °C showed magnetic saturation (M_s) values of 0.13 emu g^{-1}, 3.944 emu g^{-1}, and 11.63 emu g^{-1}, while residual magnetization (M_r) values were 0.44 emu g^{-1}, 0.85 emu g^{-1}, and 2.409 emu g^{-1}, respectively.

Notably, ferromagnetic properties were enhanced with increasing co-pyrolysis temperature and high coercivity (H_c). Table S2 shows the VSM values of all catalysts: M_s, M_r, H_c, and M_r/M_s. Fig. S10 depicts the contact angles of the catalysts, where hydrophilicity increases with increasing co-pyrolysis temperature. Fig. S1b represents the catalyst's zeta potential. Enhanced co-pyrolysis could enhance the suspension or neutrality (pH_{pzc} of 4.3) of the catalytic surface in favor of pollutant adsorption.

Fig. 2e and Fig. S1a reveal the electrochemically enhanced properties of Fe-SCS@BR700 °C, as measured by electrochemical impedance (EIS). Interestingly, with increasing co-pyrolysis temperature, the semicircle reduces, meaning the electron transfer ability increases or the charge transfer resistance decreases. Fig. S1a depicts cyclic voltammetry (CV) curves of all catalysts, which are directly proportional to the co-pyrolysis temperature of all catalysts, showing a significant current response against specific potential scan rates. Based on these observations, SCS@BR-700 °C showed the highest electron transfer ability and current response. XPS results also confirmed the EIS and CV results, due to the iron content at higher temperatures (Fig. 2c). To understand the optimum co-pyrolysis temperature, an analysis of the thermogravimetric (TG) curves of the BR, SCS, and mixture (SCS : BR) under an N_2 atmosphere was performed (Fig. S1(c) and Fig. 2(f)). The TG curve of raw BR, at 146.5 °C, showed weight loss was 5.22%, but 30.75% at 381.9 °C in the second stage, due to the leftover constituents of BR burning after anaerobic decomposition, including lignin, crystalline cellulose, and hemicellulose[30] (Fig. S1(c)). However, the most suitable co-pyrolysis temperature of BR can be considered to be 535.5 °C (14.59%) to 946.8 °C (6.82%) due to maximum reduction in weight loss. Fig. 2(f) also indicates the minimum weight loss of the raw SCS (Fig. S1(c)), which was 1.27% at 947.5 °C, mainly due to the presence of heavy metals like Fe, Ca, Si, and Al. Notably, Fig. 2(f) depicts the combined weight loss of 4.56% at 158.93 °C and 2.22% at 222.71 °C, but this suddenly decreases to 22.06% at 526.43 °C due to the carbon content of BR, before stopping at 12.56% at 716.95 °C due to the metal content of SCS. Hence, it was concluded that the mixture (SCS : BR) (1 : 5) exhibits maximum stability up to the optimum temperature of 700 °C.

TEM images, Fig. 1(g–i), show that the light blackish color layers are due to overlapping SCS and BR at various temperatures.[31] Notably, the temperatures increase resulted in more obviously overlapping SCS and BR, ultimately indicating the optimum temperature. Finally, advanced characterization confirmed a strong synergistic effect between BR and SCS nanocomposites, elucidating the underlying mechanisms and showing potential for real wastewater applications.

3.2. Catalytic ozonation degradation

3.2.1 Comparison of the catalytic performance for OFL. First, the limited adsorption potential (14.54%) was revealed for simulated urine containing OFL (Fig. S3). Hence, newly prepared novel catalysts were exposed to adsorption-enhanced catalytic ozonation degradation of simulated urine over a period of 100 minutes. Fig. 3(a and b) represents the comparative catalytic ozonation activities of all catalysts (Fe-SCS@BR-300 °C/500 °C/700 °C) under SDI and simulated urine containing OFL (20 mg L^{-1}) for comparison, respectively. Fig. 3(a) reveals that OFL (20 mg L^{-1}) was completely removed, in just 20 min, by catalysts prepared at elevated temperatures (*i.e.*, 500 °C and 700 °C) from SDI solution. Meanwhile, Fig. 3(b) shows that a similar concentration of OFL was removed (98%) over a period of 100 min from simulated urine. This scavenging effect is due to the variety of organic and inorganic constituents (*i.e.*, urea, creatinine, salts, and organic acids) in urine that can easily occupy the catalyst active sites and hinder the generation of ROS. Based on these observations, the Fe-SCS@B-700 °C catalyst was the best-performing and optimum catalyst. Finally, it was concluded that the enhanced co-pyrolysis temperature and the reaction medium's matrix could play key roles in superior synergy and pollutant degradation. For calculating the catalytic activity, relevant information is given in Section S4.

Finally, Fe-SCS@B-700 °C was successfully tested for OFL degradation under the scavenging effects of simulated urine (HCO_3^-/CO_3^{2-}), chloride (Cl^-), and ammonium (NH_4^+) until the third cycle (>75%) (Fig. S12a). Furthermore, a comprehensive comparison study based on removal efficiency confirmed its effectiveness (Fig. S13a and S14b and Table S11).

3.2.2 Performance evaluation of the fixed-bed reactor and environmental implications. Real swine wastewater challenges traditional treatments with its high levels of antibiotics, nutrients, and organics, while the proposed adsorption-assisted catalytic ozonation enhances pollutant–oxidant contact and ozone breakdown, achieving efficient degradation in a single fixed-bed reactor system (Fig. 3h and Fig. S7b). An optimum catalyst (Fe-SCS@BR-700 °C) was utilized for swine urine-manure-separated adsorption-supported ozonation, conducted over a period of 100 min under real environmental conditions, whereupon product samples were obtained. First, a QTRAP ABI-3200 system was employed to investigate toxic pharmaceutical pollutants in swine urine (Section S4, Fig. S11a and b,

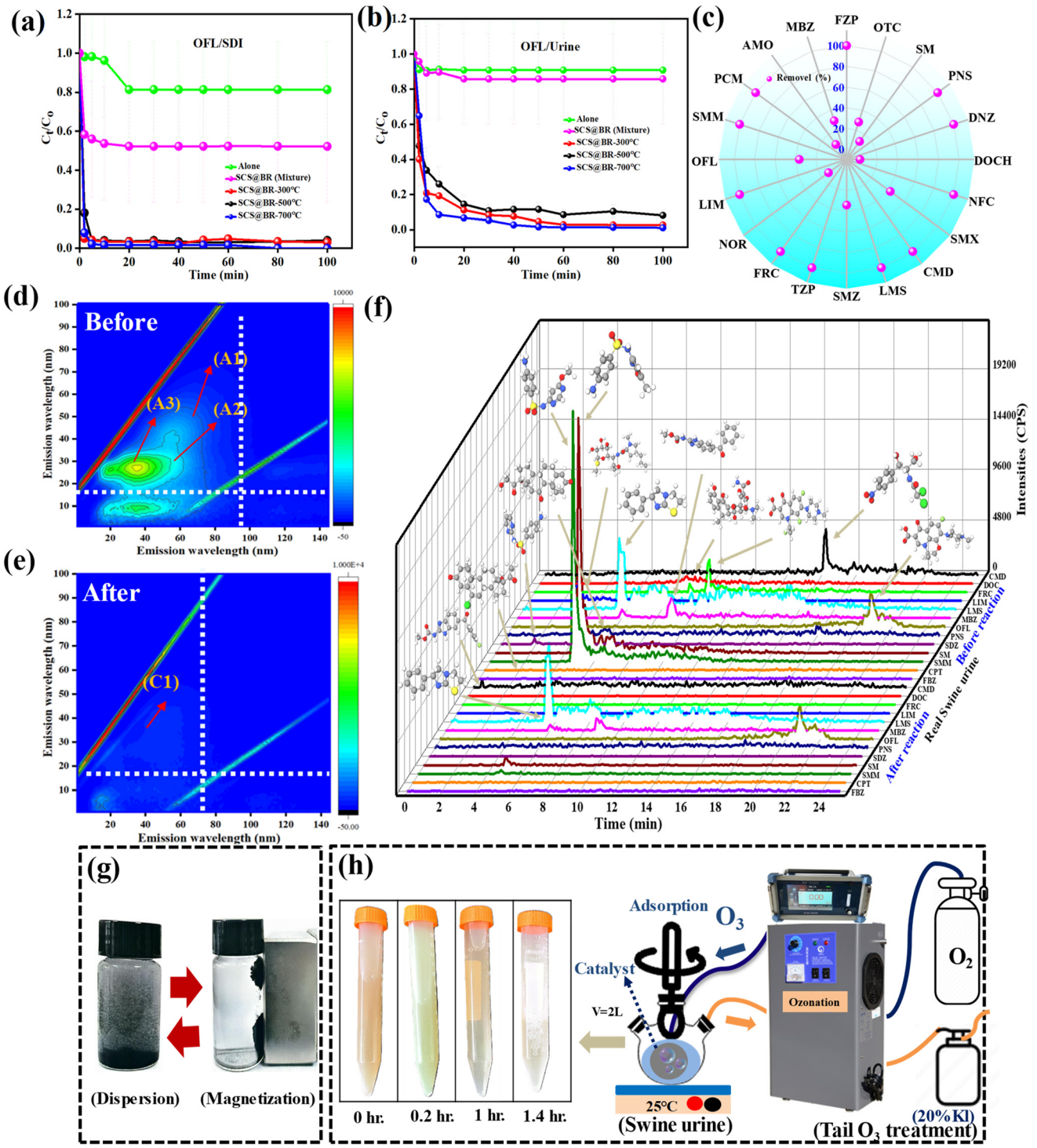

Fig. 3 Catalytic activity over different catalysts. (a) Ofloxacin (SDI water), (b) ofloxacin (simulated urine), removal efficiency of pharmaceuticals in (c) real swine urine, after the reaction, and (d and e) swine urine's 3D-EEM spectrum, before and after the reaction. (f) Pharmaceutical intensities (CPS) in real swine urine before and after the reaction, over Fe-SCS@BR-700 °C/O_3. Conditions: [OFL] = 20 mg L^{-1}, [O_3] = 5.5 ± 0.5 mg L^{-1}, [V] = 200 mL, catalyst = 0.20 g, pH (urine) = 8.85, pH (simulated) = 9.17, T = 25 °C ± 0.5 °C, time = 100 min, revolutions = 650 rpm (g and h) catalytic magnetization and lab scale plot study treatment for real swine urine. Conditions: [V] = 2 L, [O_3] = 27.5 ± 0.5 mg L^{-1}, catalyst = 2 g, pH = 8.85, T = 25 °C ± 0.5 °C, time = 100 min, revolutions = 1200 rpm.

and Tables S7a and b). To detect the cause of signal intensities, comparison with a drug library helped to identify the molecular formulas and molecular weights of the organic pollutants extracted by mass spectrometry. As per the analysis, the following compounds were successfully detected: three sulfonamides (sulfamethoxazole, sulfamonomethoxine, sulfamethazine); three quinolone antibiotics (fleroxacin, ofloxacin, norfloxacin); four antibiotics (oxytetracycline, levamisole, lincomycin, doxycycline); one antiparasitic drug (mebendazole); one sedative/hypnotic (flunitrazepam, also known as rohypnol); one central nervous system (CNS) stimulants (donepezil); one steroidal antiandrogen (chlormadinone); and one corticosteroid (prednisone) (Fig. 3f and Fig. S11a and Table S7a). After the reaction, the signals for sulfamethoxazole, sulfamethazine, sulfamonomethoxine, oxytetracycline, quinolone antibiotics (ofloxacin, fleroxacin, norfloxacin), and the antiparasitic drug (levamisole) were not detected (Fig. 3f and Fig. S11b and Table S10b). Additionally, the HPLC standard curve method helped to determine each antibiotic concentration in swine urine (Section S4). Fig. 3f shows the removal percentages of the antibiotics with the highest signal intensities after the reaction (<0.01 ppm) as follows SMX (42.70%) > OFL (36.29%) > SMZ (34.24%) > MBZ (29.36%) > OTC (28.07%) > SM (11.48%) > AMO (7.93%) > NOR (7.93%), and DOC (3.044%), meeting China's national standard (GB/T 32951-2016) for organic fertilizers,[32] while LMS, PCM, NFE, LMS, SMZ, SM, SMM, MBZ, FZP, DNZ, and PNS were not detected. Finally, the catalyst after the reaction was separated by magnetization for further use without regeneration (Fig. 3g).

Additionally, as a secondary benefit, mixed swine urine and manure were treated, resulting in reductions of P (21%), Ca (18.8%), Na (13.2%), and K (9.8%) *via* struvite crystallization and recovery by adsorption over Fe-SCS@BR-700 °C/O_3, contributing to sustainable circular agriculture innovation[33] (Fig. S5a). FTIR analysis of ozonated swine manure revealed a 35% reduction in C–H stretching (2900 cm^{-1}) and a 28% decrease in amide I band intensity (1650 cm^{-1}), indicating enhanced biogas potential through lipid degradation and reduced NH_3 toxicity risk *via* protein breakdown, respectively. Notably, the emergence of new C=O (1700 cm^{-1}) and C–O (1200 cm^{-1}) peaks indicated an increase in the formation of biodegradable intermediates[34] (Fig. S5b). This green adsorption–catalytic ozonation process not only eliminates antibiotics but also enables circular livestock waste management.

3.2.3 COD, TOC, and 3D-EEM of degraded OFL and real swine urine. To determine the optimum catalyst activity of Fe-SCS@BR-700 °C, chemical oxygen demand (COD), total organic carbon (TOC), and three-dimensional excitation–emission matrix (3D-EEM) fluorescence spectra were measured. Fig. S4(a and b) depicts significantly higher COD removal efficiency for OFL at 67.96% in SDI water as compared to that in simulated urine at 20.66% due to scavenging impacts. Fig. S4c reveals 71% COD removal for real swine urine effluents. Fig. 3c shows that the TOC removal level over Fe-SCS@BR-700 °C/O_3 from real swine urine was higher, comparatively, due to a favorable composition for microbial activity.[35] Similarly, Fig. S4(d and e) shows that Fe-SCS@BR-500 °C facilitated higher TOC removal than Fe-SCS@BR-300 °C in both solutions. After the reaction, 3D-EEMs revealed the identity of the degraded organic ingredients in real swine urine and the OFL-simulated urine.[36] Fig. 3(d and e) depicts 3D-EMM spectra of real swine urine containing complex organic substances (antibiotics, protein, humic matter, *etc.*) indicated by A1, A2, and A3 (emission wavelength x = 20–80 nm, y = 2–60 nm) that are significantly transformed into less harmful and easily degradable compounds C1 after 100 minutes, respectively. Fig. S2(a and b) indicates that the high fluorescence signals of OFL, divided into regions E, F, and G, were successfully diminished following degradation of organic pollutants in the urine environment, resulting in the emergence of a new spectral region H. Hence, it was observed that a considerable amount of organic matter was degraded successfully.

3.2.4 Factors affecting degradation by catalytic ozonation. To optimize the experimental conditions, various factors such as catalytic dose, ozone quantity, pollutant concentration, initial temperature, and pH were considered under conditions of simulated urine containing OFL. Fig. 4(a–f) shows that at the initial natural pH of the simulated urine containing OFL (9.70), catalytic removal efficiency for OFL was 91.81%. It has already been documented that catalytic ozonation is more favorable under more alkaline conditions.[37] Meanwhile, a more acidic environment could convert reactive species to weaker active species.[27] Notably, oxygen-reactive species like $^1O_2$ have a high pH tolerance, already confirmed by EPR (Fig. 6f), resulting in stable degradation of OFL in urine.[38] In Fig. 4(b), which shows pollutant loading, it can be seen that 20 mg L^{-1} (91.81%) was a more suitable dose. This is due to fewer intermediates, competition, and abundant active sites at a lower pollutant load.[39]

Fig. 4(c) shows higher degradation at 0.15 g, which is the optimum catalytic dosage. Based on this evaluation, as shown in Fig. 4(d), a concentration of 17.40 mg L^{-1} O_3 is most efficient for OFL degradation. This means that a higher O_3 dosage could increase the scavenging effects, thereby decreasing degradation.[40] Fig. 4(e) shows the critical role of temperature during degradation under a urine matrix, where an enhanced catalytic temperature of 25 °C was observed. Notably, the creatine, creatinine, and hippuric acid content of urine can directly affect the degradation. These substances are endogenous in urine and significantly affect the degradation of pharmaceuticals and other organic pollutants. Therefore, considering simulated urine, the effects of creatine, creatinine, and hippuric acid should be evaluated during the reaction. Fig. 4f reveals that these ingredients have an overall negative impact on antibiotic degradation in simulated urine due to scavenger effects.

4. Identification of ROS and active site assessment

Based on the previous results and post-reaction XPS analysis, a comprehensive degradation mechanism can be proposed.

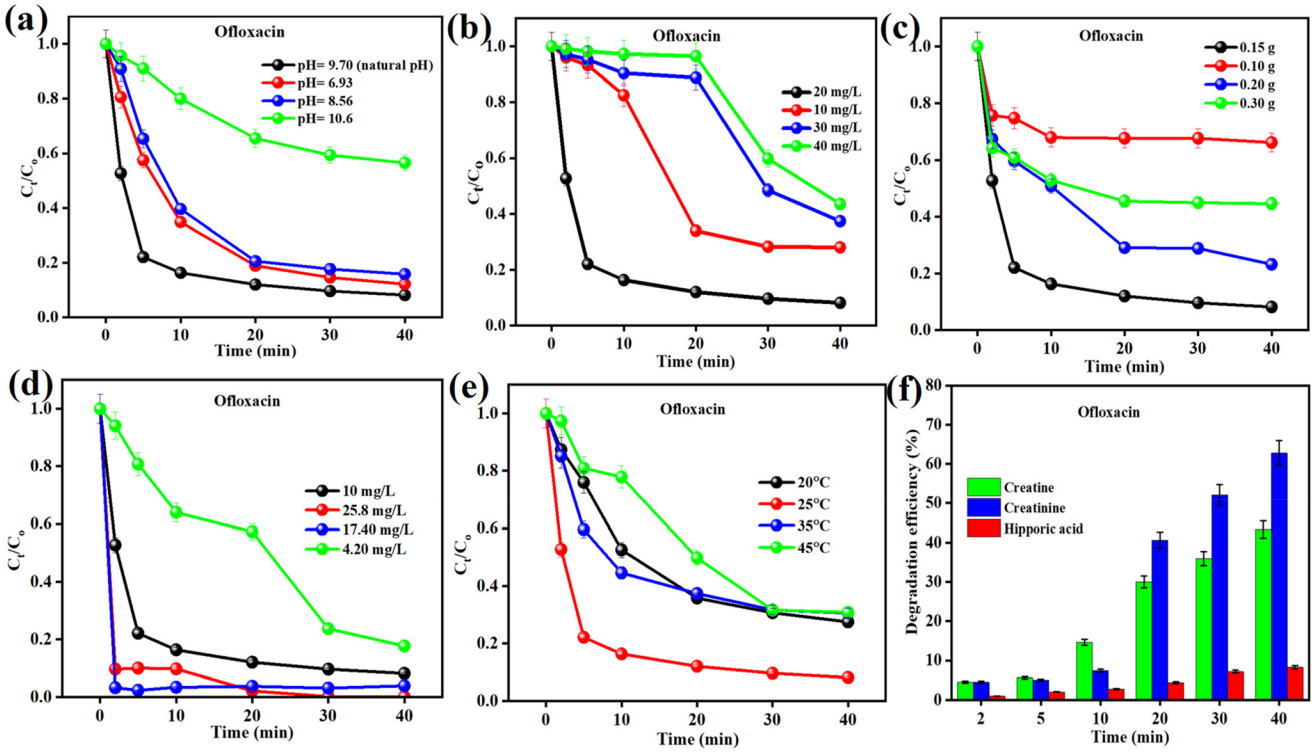

Fig. 4 Ofloxacin degradation over simulated urine under different (a) pH values, (b) pollutant load, and (c) catalytic doses, and (d–e) different ozone concentrations at different temperatures over Fe-SCS@BR-700 °C. (f) Effects of creatine, creatinine, and hippuric acid. Conditions: [V] = 200 mL, time = 100 min, revolutions = 650 rpm, while [O_3], catalyst, pH, and temperature; [OFL] concentrations were kept changing.

Oxygen-containing functional groups play a crucial role as active sites for ROS production in O_3 decomposition of carbon-based materials. Fig. 5(a–c) shows XPS peaks before and after the catalytic reaction. Specifically, Fig. 5(a) shows a reduction in the C 1s signals after the reaction, corresponding to C=C and C–C bonds with relative abundances decreasing from 18.32% to 20.35% in SDI water, and from 59.28% to 52.15% in simulated urine, while enhancement of the carbonyl group (C=O) signal was observed. The C=C and C–C bonds acted as π-electron donors, while OH–C=O and π–π electron variations were detected, indicating successful reaction outcomes. Fig. 5b reveals that metal oxide (Fe_2O_3, Fe_3O_4, $CaCO_3$, SiO_2, and calcite) plays a significant role, and that the C–C bond plays a donor role by enhancing the C=O bond. Fig. 5c shows the distinct peaks of Fe-2p (Fe-$2p_{2/3}$ to Fe-$2p_{1/2}$) before and after the reaction. Notably, Fe^0 (3.39%) was formed due to the conversion of Fe_2O_3 and Fe_3O_4 at an enhanced carbothermal temperature,[41] as previously confirmed by XRD and FTIR (Fig. 2(a and b)). Moreover, before the reaction, peaks of Fe-$2p_{3/2}$ were divided into Fe^{2+} (707.7 eV) (18.62%) and Fe^{3+} (710.3 eV) (25.03%), while peaks of Fe-$2p_{1/2}$ were divided into Fe^{2+} (721.7 eV) (10.0%) and Fe^{3+} (722.9 eV) (28.43%). After the reaction, significantly distinct changes in the peaks were seen in both water matrices (Fig. 5d). In SDI water, Fe-$2p_{3/2}$ (Fe^{2+} and Fe^{3+}) peaks changed from 18.62% and 25.03% to 28.73% and 20.87%, respectively, while in the urine solution, Fe^{2+} (14.34%) and Fe^{3+} (29.14%) peak changes were observed. Interestingly, Fe^0 acted as an electron donor, confirmed by EIS (Fig. 2e), and facilitated a redox reaction to generate ROS. Finally, these novel mechanistic insights revealed that iron-rich nano-composites like SCS@BR-700 °C can dominate redox reactions in a real urine environment. Notably, these findings align with the experimental results (Fig. 3a and b), which mean these breakthrough results can unlock the potential for real-world antibiotic (*e.g.*, OFL) remediation in challenging waste streams.

Scavenger experiments (Fig. 5e) were performed in the Fe-SCS@BR-700 °C/O_3 system under urine conditions to determine the level of O_3 activation in ROS generation. *tert*-Butyl alcohol (TBA) indicated the kinetics of $^{\bullet}OH$ ($k_{\cdot OH\ TBA}$ = (3.8–7.6) × 10^8 M^{-1} s^{-1}), while benzoquinone (BQ) trapped the $O_2^{\bullet-}$ ($k_{O_2^{\bullet-}\ BQ}$ = 1.0 × 10^9 M^{-1} s^{-1}).[40] Importantly, DMSO (5,5-dimethyl-1-pyrroline *N*-oxide) scavenged $O_2^{\bullet-}$, $^{\bullet}OH$ and $^1O_2$. The results in Fig. 5e confirm that all ROS hindered the reaction, and scavenging of $O_2^{\bullet-}$ (OFL = 58.34%) revealed their serious impact during antibiotic degradation under urine conditions. Hence, $O_2^{\bullet-}$ confirmed its critical role in the Fe-SCS@BR-700 °C/O_3 system in simulated urine containing OFL. EPR spin-trapping was performed for 5–10 min under simulated urine conditions to detect the presence of ROS using DMPO and TEMPO. Fig. 5(f and g) shows that distinct, relatively strong signals of $O_2^{\bullet-}$ and $^{\bullet}OH$ were observed. However, the limited signals of $^1O_2$ (Fig. 5h) indicate significant removal (83.12%) upon TBA scavenging, whereas $O_2^{\bullet-}$ signals remained relatively strong and persistent in the urine environment.

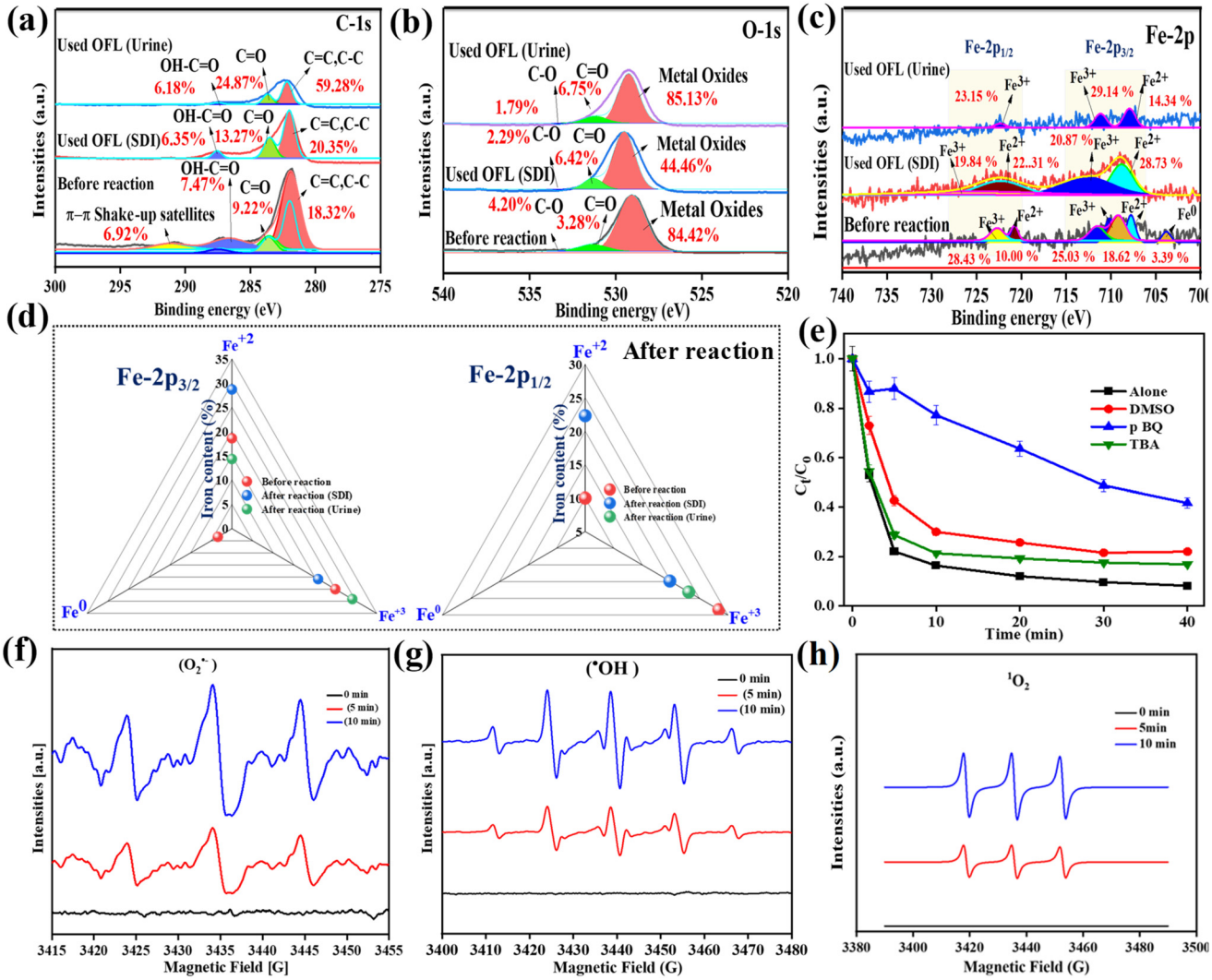

Fig. 5 XPS of Fe-SCS@BR-700 °C before and after the reaction under SID and simulated urine. (a) C-1s, (b) O-1s, and (c) Fe-2p. (d) Iron content changes (%). Scavenger tests for OFL degradation in simulated urine (e) and (f–h) EPR peaks in a urine environment (OFL) over Fe-SCS@BR-700 °C/O_3. Conditions: [OFL] = 20 mg L^{-1}, [V] = 200 mL, [O_3] = 5.5 ± 0.5 mg L^{-1}, catalyst = 0.2 g, pH (simulated urine) = 9.17, scavengers' concentration = 0.2 mM, T = 25 °C ± 0.5 °C, time = 40 min, revolutions = 650 rpm.

Interestingly, the above-mentioned mechanism revealed the electron donor and redox reaction ability of Fe-2$p_{3/2}$, Fe-2$p_{1/2}$, and Fe^0, which played a vital role in ROS generation.

5. Catalytic degradation mechanism verified by DFT calculations

To elucidate the above-mentioned ROS and active site results, a DFT study was performed to reveal adsorption-promoted synergies between O_3 and the Fe content of SCS compared to the performance of active sites of various functional groups for OFL degradation. Fig. S5c depicts the FMO of the raw BR and Fe-SCS@BR-700 °C after co-pyrolysis, confirming electron transfer ability.

Fig. 6a reveals that the sp^2-hybridized carbon content of Fe-SCS@BR-700 °C can facilitate the transformation of delocalized π electrons. This transition likely occurs from the LUMO (−0.2341 eV) of the sp^2-hybridized orbital to its HOMO (−0.30911 eV) due to the HOMO–LUMO gap. Finally, direct ozonation could occur between ofloxacin and O_3.[42] Fig. 6c shows representations of DFT calculations for different adsorption values of Fe-SCS@BR-700 °C over O_3. All adsorption models were established based on the XPS and FTIR results of Fe-SCS@BR-700 °C. Optimization was performed using the Forcite model to calculate energies, and additional adsorption locator models having an initial adsorption distance of 10 Å were applied to estimate the total energy of the particular adsorption model separately. As per the following equation (eqn (3)), different models of Fe-SCS@BR-700 °C/O_3 (ozone E_{ads} = 42.38 kcal mol^{-1}) were calculated (Table S3):

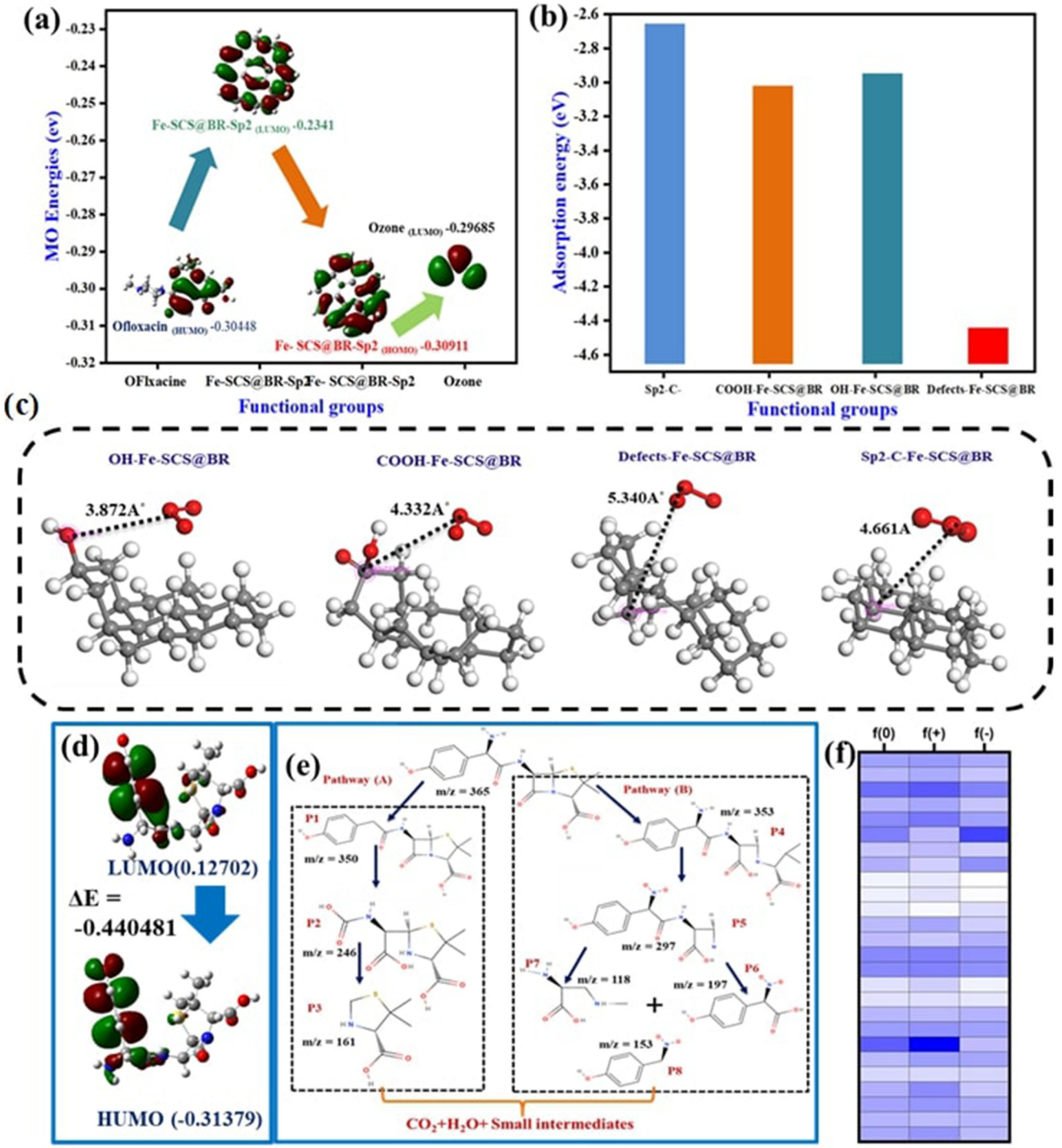

Fig. 6 (a and b) Direct ozonation (FMO structures of the raw Fe-SCS@BR after co-pyrolysis and ozone role for electron transfer for OFL), (c) adsorption energies and adsorption distance of ozone over different models of Fe-SCS@BR-700 °C, (d) the HUMO and LUMO of amoxicillin (easily degradation sites), (e) the degradation pathway of amoxicillin (recalcitrance then other antibiotics) in a urine environment, over Fe-SCS@BR-700 °C/O_3, and (f) AMO Fukui indices.

$$E_{ads} = E_{adsorption\ system} - E_{catalyst} - E_{O_3} \quad (3)$$

All adsorption energies and distances of O_3 over the surface functional groups of SCS@BR-700 °C are shown in Table S3. Adsorption energy values vary from −2.75 eV to −4.50 eV, which means strong adsorption of O_3 over Fe-SCS@BR-700 °C is due to exothermic interactions. This means that the highest adsorption energy of O_3 over defects-Fe-SCS@BR-700 °C was

−4.50 eV, while having the longest adsorption distance at 5.340 Å. It has been shown that interaction at defect sites allows for adsorption over a longer distance while still maintaining a strong interaction.[43] Fig. 6d confirms the possibly different adsorption distances, verifying the adsorption of O_3 over different Fe-SCS@BR-700 °C models during the reaction.

6. DFT calculations and the possible degradation pathways

The Fukui function and DFT calculations were performed to investigate the vulnerable reactive sites revealed by the HUMO and LUMO of Amoxicillin (AMO) and OFL that possibly caused degradation over Fe-SCS@BR-700 °C/O_3 Fig. 6(d–f), and Fig. S6 respectively. Fukui indices of AMO are shown in Fig. 6(f) and Tables S4–S6. It has already been shown that atoms with higher values of f^0 are more susceptible to ROS.[44] It was observed that OFL has O3, O5, N6, C14, and C20 (Fig. S6), while AMO has S1, N4, C8, C11, and C12 as more susceptible atoms to be attacked by ROS, as shown by the color clouds (Fig. 6d). Pathway study targeted AMO (7.9%) (Fig. 3c) for persistence instead of OFL. For AMO, possible degradation pathways were investigated, and samples were collected over Fe-SCS@BR-700 °C/O_3 and filtered using a 45 μm filter at a particular time. Later on, liquid chromatography-mass spectrometry (LC-MS) was performed to reveal the intermediates (Fig. S9).

Fig. 6(e) shows the possible AMO degradation pathways based on DFT and the identified intermediates. In pathway (A), P1 (m/z = 350) was formed due to higher f^0 N9 values (0.068) (Table S4), where $O_2^{\bullet-}$ could attack $^1O_2$, while the C═O group was broken near the benzene and β-lactam rings to generate P2 (m/z = 246).[45] Besides the limited $^{\bullet}OH$ (Fig. 6(a and b)), it could still cause the conversion of P2 (m/z = 246) to intermediate P3 (m/z = 161), finally reaching mineralization of intermediates to CO_2 and H_2O and small intermediates. Pathway (B) shows the AMO degradation route by cleavage of the amide bond and a decarboxylation reaction. S1 of AMO, with a higher value of f^0 (0.048) (Tables S4–S6), was susceptible to free radicals like $O_2^{\bullet-}$ and $^1O_2$. Subsequently, P4 to P5 intermediates could be converted due to the attack of ROS by O_3 over Fe-SCS@BR-700 °C on the benzene group, and oxidation of the phenolic hydroxyl group. Furthermore, under the combined attack of $^{\bullet}OH$, $O_2^{\bullet-}$, and $^1O_2$, decarboxylation, amide bond oxidation, and amino group oxidation will move towards CO_2 and H_2O and small intermediates.[45]

7. Proposed reaction mechanism

Based on the investigation of active site changes during Fe-SCS@BR-700 °C/O_3 degradation processes, before and after the reaction, as revealed by XPS, a possible reaction mechanism for the removal of OFL from the urine matrix has been proposed (Scheme 1). Heterogeneous catalytic ozonation degradation of organic compounds has several pathways to decompose the O_3.[46] The significant presence of superoxide $O_2^{\bullet-}$, $^1O_2$, and $^{\bullet}OH$ was detected by scavenger and EPR tests. Organic urine substances like creatine, creatinine, and hippuric acid can hinder the catalytic reaction due to scavenging effects (Fig. 4(d and e)).[27] Based on the DFT adsorption study of O_3 over the Fe-SCS@BR-700 °C surface (Fig. 6c), defects in the structure are directly responsible for oxygen-rich species generation, due to enhanced electron transfer.[47] O_3 activation could be determined by the free-flow π-electron produced by the sp^3 carbon-abundant material[48] (eqn (4)–(9)):

$$\text{Carbon–}\pi + 2H_2O \rightarrow \text{carbon–}H_3O + {}^{\bullet}OH \quad (4)$$

$$O_3 + OH \rightarrow {}^{\bullet}HO_2 + O_2^{\bullet-} \quad (5)$$

$${}^{\bullet}HO_2 \rightarrow O_2^{\bullet-} + H^+ \quad (6)$$

or

$$O_3 + H_2O \rightarrow 2{}^{\bullet}OH + O_2 \quad (7)$$

$$O_3 + OH^- \rightarrow O_2^- + HO_2^- \quad (8)$$

$$O_3 + {}^{\bullet}OH \rightarrow O_2 + HO_2^{\bullet} \leftrightarrow O_2^{\bullet-} + H^+ \quad (9)$$

Based on the XPS spectra before and after the reaction, it was investigated whether oxygen-containing functional groups like C═O, $^{\bullet}OH$, and COOH, and sp^2-hybridized orbital or metal ions like Fe^0, Fe^{2+}, or Fe^{3+} (Fig. 7) could enhance the O_3 depletion and generation of ROS like $^{\bullet}OH$, $^1O_2$, and $O_2^{\bullet-}$ over Fe-SCS@BR-700 °C.[49] (i) As per eqn (1) and (2), the presence of Fe^0 ions in the Fe-SCS@BR-700 °C was due to iron oxide species at higher temperatures with carbon substances. (ii) These species can generate Fe^{3+} and Fe^{2+} (eqn (10)–(12)), where trivalent iron species like Fe^{3+} can directly react with soluble O_3 and donate free electrons towards O_3, resulting in $O_2^{\bullet-}$, $^1O_2$ and $^{\bullet}OH$ (eqn (5) and (6)).[49] Meanwhile, $O_2^{\bullet-}$ can react directly with Fe^{3+}, generating $^1O_2$.

Moreover, the standard reduction potential (E_0) (Fe^{2+}/Fe^{3+}) = 0.77 V is lower than that of O_3 (E_0 (O_3/O_2)) = 2.07 V.[50] Therefore, O_3 will be split into ROS due to the iron species and could ultimately react with the OFL, resulting in CO_2 and water:

$$\equiv Fe^0 + 2Fe^{3+} \rightarrow 3Fe^{2+} \quad (10)$$

$$\equiv Fe^{3+} + O_2^{\bullet-} \rightarrow Fe^{2+} + H^+ + {}^1O_2 \quad (11)$$

$$\equiv Fe^{3+} + O_3 + H_2O \rightarrow Fe^{2+} + 2OH + O_2^{\bullet-} \quad (12)$$

(iii) It has been documented that oxygen-rich species such as COOH could donate electrons to O_3, resulting in $^{\bullet}O_3^-$, $^{\bullet}OH$, and $O_2^{\bullet-}$ (eqn (13)):

$$3COOH + 2O_3 \rightarrow 3COO^{\bullet} + 3O_2^{\bullet-} + 3H^+ \quad (13)$$

(iv) Furthermore, another C═OH group could donate free electrons to O_3, resulting in $O_2^{\bullet-}$, $O_3^{\bullet-}$ and $^{\bullet}OH$ (eqn (14)):

$$C{=}OH + O_3 \rightarrow O_3^{\bullet-} + C{=}O^{\bullet} + H^+ \quad (14)$$

As per the results, Fe-SCS@BR-700 °C/O_3 degradation (Fig. 3a and b) was greater than single ozonation due to abun-

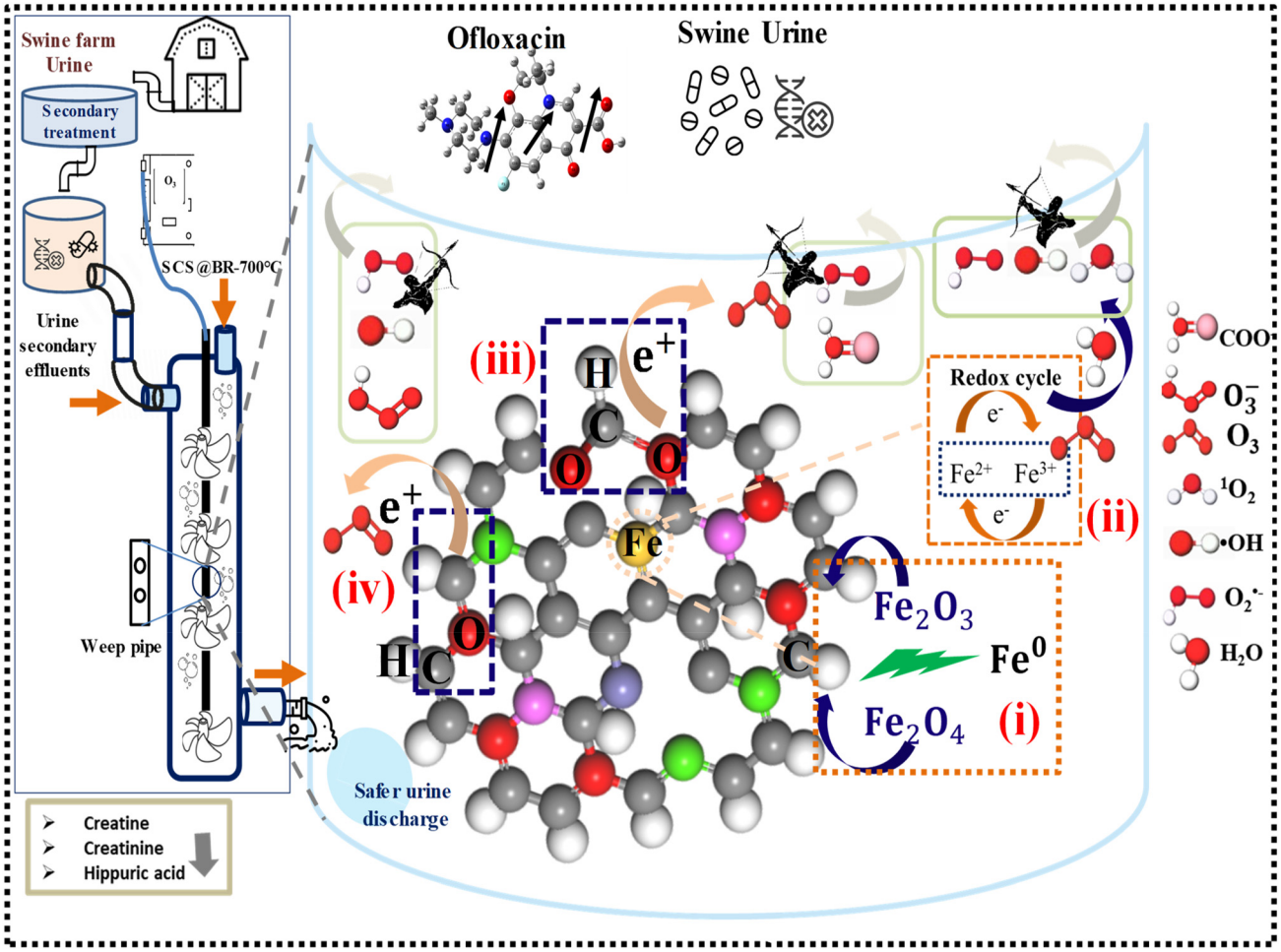

Scheme 1 Mechanistic illustration of the catalytic ozonation of OFL and real swine urine's pharmaceutical degradation over the Fe-SCS@BR-700 °C/O_3 system.

dant ROS. Hence, DFT revealed the possible adsorption of O_3 over the surface groups of Fe-SCS@BR-700 °C to produce ROS, as confirmed by scavenger test, EPR, and XPS results before and after the reaction. Consequently, Fe-SCS@BR-700 °C successfully activated O_3 for ROS generation, and is possibly involved in catalytic ozonation degradation of OFL into smaller intermediates, CO_2, and H_2O. Furthermore, a vertical economic fixed-bed design for adsorption support ozonation for small pigsties was proposed for better mixing and efficiency.

8. Environmental implications and evaluation assessment

8.1 Biological toxicity and LCA assessment over Fe-SCS@BR@700 °C

Evaluating heavy metal leaching for steel converter slag-based catalysts like Fe-SCS@BR-700 °C should be of primary concern for biological toxicity and impact assessment. To determine the safest optimum catalytic dose of the Fe-SCS@BR-700 °C against an OFL solution, various doses of 0.1 g, 0.2 g, and 0.3 g were tested (Fig. 7a).

Samples were subsequently collected for ICP-MS. Most abundant toxic metals leaching over the catalyst to the solution, such as Al, Fe, and Ca, were evaluated against the World Health Organization (WHO) and United States Environmental Protection Agency (USEPA) standards for drinking water. It was seen that Fe and Al leaching values were 0.1 mg L^{-1}–0.3 mg L^{-1}, and 0.75 mg L^{-1}, respectively, both below the safe limit per WHO and USEPA guidelines for aquatic life and ambient water quality. Notably, Ca leaching was favorable for an aquatic ecological environment. Finally, based on metal leaching results, 0.1 g–0.2 g of the catalysts were considered environmentally benign. Consequently, the biological toxicity assessment of the treated OFL solution and intermediates of the ozonated urine was practically investigated by germinating wheat seeds (Fig. 7c). Based on observations, germination under real soil conditions, where 95.5% growth occurred within 5 days, followed irrigation with SDI water. No growth was observed due to the OFL contamination. However, after treatment of the contaminated water over Fe-SCS@BR-700 °C/O_3, significant recovery (85.5%) of the grain's

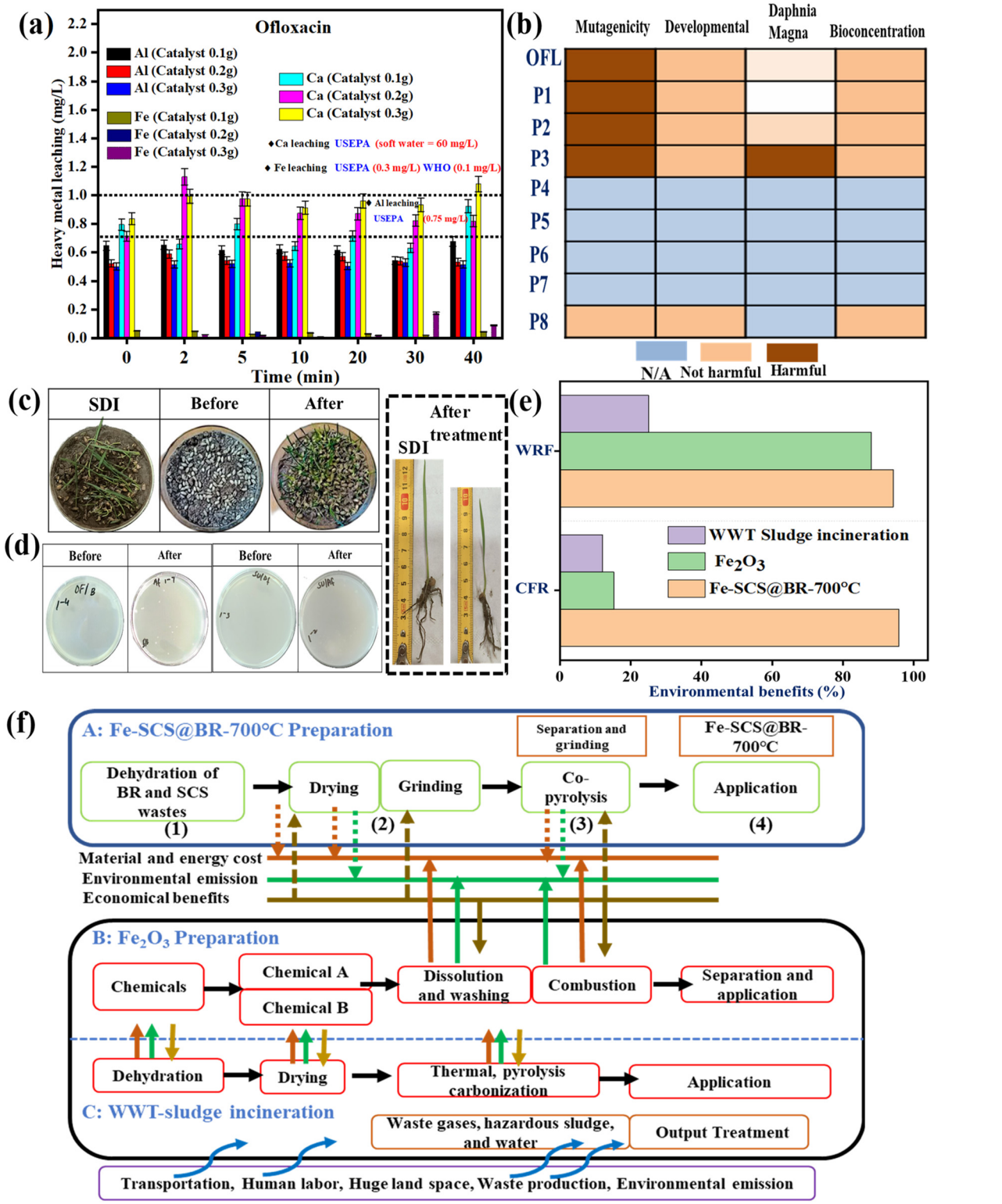

Fig. 7 Optimum Fe-SCS@BR-700 °C/O_3 dosage. (a) Heavy metal leaching, (b) toxicity assessment and (c) wheat grain growth under ozonated urine and SDI. (d) *Escherichia coli* (*E. coli*) growth experiment under OFL and swine urine, (e) environmental benefits, and (f) system boundaries for waste-based Fe-SCS@BR-700 °C, chemically synthesized Fe_2O_3, and sludge disposal. Conditions: [OFL] = 20 mg L^{-1}, [V] = 200 mL, [O_3] = 5.5 ± 0.5 mg L^{-1}, catalyst = (0.1–0.3) g, pH (urine) = 8.85, pH (simulated) = 9.17, T = 25 °C ± 0.5 °C, time = 100 min, revolutions = 650 rpm; for (c and d), see details given in Text S6.

growth was observed under real soil conditions. It was observed that the biological toxicity after treatment was significantly reduced. Additionally, *Escherichia coli* (*E. coli*) growth by Petri plate experiments over OFL and swine urine before and after catalytic ozonation degradation was performed over 12 h (Section S6). As per analysis (Fig. 7d), it was seen that *E. coli* growth was inhibited before the reaction due to the presence of antibiotics or organic pollutants, but after the reaction, significant growth was observed. Finally, organic pollutants in swine urine were successfully eliminated over Fe-SCS@BR-700 °C/O_3. Notably, Fe-SCS@BR-700 °C also showed a satisfactory performance under real water conditions (Fig. S13b). Moreover, ozonated urine successfully met the water quality standard parameters of both international organizations (Fig. S14). Hence, the novel nano-composite proved to be greener and multi-functional for the degradation of OFL and complexes of a real swine urine matrix (Fig. 7e).

To meet the targets of carbon dioxide emission reduction by 2030 and achieve carbon neutrality by 2060, as announced by the 75th UN General Assembly in 2020, a potential solution in Fe-SCS@BR-700 °C has been proposed with results of its life cycle assessment analysis (LCA) (Fig. 7e and f) (Section S7). To evaluate all possible environmental, economic, and social benefits, studies have been performed (Tables S9–11). Although the data from the analysis were not perfect, it can be easily concluded that the synthesis waste-based Fe-SCS@BR-700 °C catalyst has significant environmental and economic benefits compared to chemically synthesized Fe_2O_3 and sludge incineration. Based on these results, 1 ton of Fe-SCS@BR-700 °C costs \$220, while only 0.4 tons of Fe_2O_3 costs \$920. Finally, it was seen that waste-based catalysts not only address the waste reduction factor (WRF) and carbon footprint reduction (CFR) comparatively (Fig. 7e), but also reduce the cost associated with sludge incineration and disposal. Finally, synthesizing these catalysts from a combination of organic waste and exogenous metals obtained from industrial metal residues could be extended to various industrial and agricultural waste products, to reveal the real potential for upcycling hazardous wastes for practical environmental remediation. Furthermore, with respect to calculations, CO_2 equivalents were avoided by using a waste-based Fe-SCS@BR-700 °C catalyst, while comprehensive calculations were performed as per the standard methods discussed in Section S7 (1–5) (i), (ii) and (iii), and comprehensive analysis of the results as mentioned in Tables S12(i), (ii) and (iii) was completed. Finally, it was concluded that Fe-SCS@BR-700 °C achieves a net carbon saving of over 16 000 kg of CO_2 per 0.4 kg batch, resulting in a 222 : 1 carbon savings ratio, which means every 1 kg of carbon invested saves 222 kg of emissions. It is a tremendously effective way to reduce emissions. These advantages show the Fe-SCS@BR700 °C catalyst's strong potential for real-world adoption.

8.2 Performance comparison, safer disposal, and installation costs

The Fe-SCS@BR-700 °C catalyst showed a satisfactory performance compared to that of commercially available catalysts like Fe_2O_3, Fe_3O_4, MnO_2, and TiO_2 or other waste-based catalysts (Fig. S13a and Table S15b). Importantly, when considering safe disposal of the utilized Fe-SCS@BR-700 °C, washing the catalyst with a polar solvent like ethanol is recommended to extract organic pollutants.[34] Sodium silicate (Na_2SiO_3) was also recommended to reduce the heavy metal leaching risk.[35] These steps could effectively prevent the risk of heavy metal leaching and release of antibiotics from the used catalyst. Importantly, installation of an adsorption-assisted, catalytic, efficient ozonation degradation system powered by solar energy offers a cost-effective solution for swine urine treatment at small and medium-scale pig farms. The Fe-SCS@BR-700 °C catalyst can be prepared in a laboratory at an estimated cost of \$0.0725 per g. For 400 L of urine (200 pigs), 300 g of Fe-SCS@BR-700 °C will be utilized daily. Furthermore, comprehensive analysis of estimated system installation costs and cost comparisons for the proposed system are shown in Tables S13a and b. Additionally, Tables S14a–c detail the catalyst preparation cost based on efficiencies, and stability comparisons with other catalysts/technologies. Additionally, comprehensive comparison of *E*-factor and real swine urine treatment was performed (Tables S15a and b). Finally, it was concluded that this proposed system combines low costs, high efficiency, and environmental benefits, making it ideal for small- and medium-sized industrial applications.

9. Conclusion

In summary, this study presents a novel and economical Fe-SCS@BR-700 °C nano-composite as an efficient catalyst that was successfully prepared by one-pot co-pyrolysis of BR and SCS and thoroughly investigated. By leveraging the unique synergistic effects following component integration at higher pyrolysis temperatures (*i.e.*, 700 °C) as revealed by characterization studies, such as uniform iron species, excellent acceleration of O_3 decomposition, and electron transfer, optimum ROS generation was achieved. Furthermore, due to the combined effect of adsorption-enhanced efficient ozonation, Fe-SCS@BR-700 °C not only significantly degraded OFL in simulated urine, but also eliminated organic pollutants from real swine urine, including various toxic antibiotics under different experimental settings. Enhanced degradation of real swine urine was confirmed by COD and TOC, and 3D-EEM for a small pigsty. Meanwhile, $O_2^{\bullet-}$ showed a significant role compared to $^{\bullet}OH$ and $^1O_2$, confirmed by scavenging and EPR results. Similarly, a DFT study has verified the presence of active sites on Fe-SCS@BR-700 °C that facilitate both direct and indirect ozonation *via* electron transfer, and identified OFL's molecular sites vulnerable to attack by ROS, particularly $O_2^{\bullet-}$. Finally, the proposed mechanism revealed a unique synergy for O_3 decomposition, an abundance of active sites (Fe^0, Fe^{2+}, or Fe^{3+}), and mass transfer due to adsorption-promoted enhanced ozonation. Moreover, safer catalytic dosage for effluent and after-reaction usage for practical environmental applications like wheat grain and *E. coli* growth under

real-world conditions was successfully investigated. Furthermore, performance assessments and cost analyses indicated that the technology offers unprecedented dual benefits, offering a promising and sustainable green solution for small pigsties to significantly remove pharmaceuticals from swine urine and to meet national livestock wastewater discharge regulations. This could be an effective economic strategy to utilize hazardous industrial waste products in the context of real environments, such as fresh water, and resource utilization.

Conflicts of interest

There are no conflicts to declare.

Abbreviations

BR	Biogas residue
SCS	Steel converter slag
EDX	Energy-dispersive X-ray spectroscopy
FTIR	Fourier transform infrared spectrometer
$O_2^{\bullet-}$	Superoxide radical
$^1O_2$	Singlet oxygen
$^{\bullet}OH$	Hydroxyl radical
PBQ	*para*-Benzoquinone
ROS	Reactive oxygen species
SEM	Scanning electron microscopy
TBA	*tert*-Butyl-alcohol
XPS	X-ray photoelectron spectroscopy
XRD	X-ray diffraction
XRF	X-ray fluorescence
AMO	Amoxicillin
OFL	Ofloxacin
OTC	Oxytetracycline
NOR	Norfloxacin
SMZ	Sulfa-methazole
MBZ	Mebendazole
SM	Sulfacetamide
DOC	Doxycycline hydrochloride
SMX	Sulfamonomethoxine
HPLC	High-performance liquid chromatography
QTRAP	Triple quadrupole liquid chromatography-mass
ABI-3200	spectrometry
LC-MS	Liquid chromatography-mass spectrometry
ICP-MS	Inductively coupled plasma mass spectrometry
LCA	Life cycle assessment
WRF	Waste reduction factor
CFR	Carbon footprint reduction

Data availability

The data that support the findings of this study will be made available upon reasonable request.

Supplementary information (SI) is available. Supplementary Information provides systematic synthesis, Analytical methods, characterization, mechanistic data (LC–MS, EPR, quenching), DFT, pilot-scale study parameters, and raw datasets. See DOI: https://doi.org/10.1039/d5gc04029a.

Acknowledgements

This work was supported by the Science and Technology Project of Fujian Province (2023T3011, 2023T3033 and 2024T3061), the Collaborative Innovation Platform Program of Fu-Xia-Quan National Innovation Demonstration Zone (3502ZCQXT2022004), and the Youth Science and Technology Innovation Program of Xiamen Ocean and Fisheries Development Special Funds (23YYST061QCA09).

References

1 L. Hao, J. Yan, J. Guo, N. Wang and M. Zeng, *J. Environ. Chem. Eng.*, 2025, **13**, 115546.
2 T. P. Van Boeckel, J. Pires, R. Silvester, C. Zhao, J. Song, N. G. Criscuolo, M. Gilbert, S. Bonhoeffer and R. Laxminarayan, *Science*, 2019, **365**, eaaw1944.
3 H. Bao, Z. Chen, Q. Wen, Y. Wu and Q. Fu, *Bioresour. Technol.*, 2024, **393**, 130127.
4 K. Zhang, R. Ruan, Z. Zhang and S. Zhi, *Sci. Total Environ.*, 2022, **847**, 157688.
5 Y. Yu, N. Jiang, Y. Zhou, F. Huang, Y. He and Y. Zhang, *J. Environ. Manage.*, 2025, **373**, 123960.
6 B. Li and T. Zhang, *Water Res.*, 2012, **46**, 3703–3713.
7 K.-F. Yu, P. Li, H. Li, B. Zhang, J. Yang, F.-Y. Huang, R. Li and Y. He, *J. Hazard. Mater.*, 2021, **406**, 124295.
8 C. Liang, D. Wei, S. Zhang, Q. Ren, J. Shi and L. Liu, *Ecotoxicol. Environ. Saf.*, 2021, **210**, 111885.
9 J. Wang, Z. Yu, T. Zhao, Y. Song, H. Liu, J. Hou and P. Yu, *Appl. Surf. Sci.*, 2025, **709**, 163837.
10 B. Chen, Y. Zhu, M. Wu, Y. Xiao, J. Huang, C. Lin and B. Weng, *Water*, 2024, **16**, 661.
11 A. Reza and L. Chen, *Environ. Chem. Lett.*, 2022, **20**, 1863–1895.
12 H. Wu and C. Vaneeckhaute, *Chem. Eng. J.*, 2022, **433**, 133664.
13 B. B. Garcia, G. Lourinho, P. Romano and P. S. D. Brito, *Heliyon*, 2020, **6**, e03293.
14 J. Liu, X. Bai and Y. Bai, *Water Cycle*, 2024, **5**, 278–285.
15 H. Kong, K. Luo and Z. Yong, *Waste Manage.*, 2024, **180**, 36–46.
16 M. Stefaniuk and P. Oleszczuk, *J. Anal. Appl. Pyrolysis*, 2015, **115**, 157–165.
17 Y. Wang, G. Yu, S. Xie, R. Jiang, C. Li and Z. Xing, *Fuel*, 2023, **353**, 129185.
18 G. P. Muthukutti, M. K. Singh, S. K. Palaniappan, K. Vijayananth, S. M. Rangappa and S. Siengchin, *Chem. Eng. J.*, 2025, **512**, 162344.

19 W. Xu, S. Dong, H. Cheng, S. Giannakis, X. Lu, Z. He, D. Wang, S. Song and J. Ma, *Chem. Eng. J.*, 2025, **513**, 162624.
20 L. Li, Y. Hua, S. Zhao, D. Yang, S. Chen, Q. Song, J. Gao and X. Dai, *ACS ES & T Eng.*, 2023, **3**, 1083–1097.
21 K. Xu, Q. Lin, X. Fan, J. Zheng, Y. Liu, Y. Ma and J. He, *Chem. Eng. J.*, 2023, **460**, 141578.
22 Y. Wang, X. Liu, Z. Cao, W. Zhang and Y. Xue, *Mater. Lett.*, 2021, **304**, 130734.
23 J. Li, L. Pan, G. Yu, S. Xie, C. Li, D. Lai, Z. Li, F. You and Y. Wang, *Sci. Total Environ.*, 2019, **654**, 1284–1292.
24 T. Jiang, B. Wang, M. Hassan and Q. Zou, *Carbon Res.*, 2024, **3**, 78.
25 X. Li, H. Liu, Y. Zhang, J. Mahlknecht and C. Wang, *J. Environ. Manage.*, 2024, **352**, 120051.
26 R. Sun, R. Huang, J. Yang and C. Wang, *Chemosphere*, 2021, **285**, 131560.
27 X. Kang, L. Wang, J. Song and Q. Zhang, *Chem. Eng. J.*, 2024, **493**, 152588.
28 Q. Yu, G. Liu, J. Shi, T. Wen and L. Li, *J. Environ. Chem. Eng.*, 2022, **10**, 108553.
29 C. Fang, L. Nie, H. Chen and Y. Yang, *J. Water Process Eng.*, 2024, **63**, 105434.
30 V. Benavente, S. Lage, F. G. Gentili and S. Jansson, *Chem. Eng. J.*, 2022, **428**, 129559.
31 A. Srikhaow, C. Chuaicham, J. Trakulmututa, K. Shu and K. Sasaki, *Sustainable Energy Fuels*, 2024, **8**, 3065–3076.
32 X. Li, J. Lan, Y. Zhang, P. Chen, S. Ding, M. Nie and S. Li, *Materials*, 2025, **18**, 3045.
33 P. Zhang, W. Wei, Y. Shang and B.-C. Ye, *Bioresour. Technol.*, 2023, **385**, 129421.
34 K. Wang, C. He, S. You, W. Liu, W. Wang, R. Zhang, H. Qi and N. Ren, *J. Hazard. Mater.*, 2015, **300**, 745–753.
35 E. Baumgarten, M. Nagel and R. Tischner, *Appl. Microbiol. Biotechnol.*, 1999, **52**, 281–284.
36 R. Yuan, Y. Qin, C. He, Z. Wang, L. Bai, H. Zhao, Z. Jiang, L. Meng and X. He, *Arabian J. Chem.*, 2023, **16**, 104415.
37 A. Behnami, J.-P. Croué, E. Aghayani and M. Pourakbar, *RSC Adv.*, 2021, **11**, 36965–36977.
38 J. Sun, H. Wu, C. Fu, C. Zhang, Z. Hu and M. Zhou, *Appl. Catal., B*, 2024, **351**, 123976.
39 E. Issaka, J. N.-O. Amu-Darko, S. Yakubu, F. O. Fapohunda, N. Ali and M. Bilal, *Chemosphere*, 2022, **289**, 133208.
40 M. Noman, G. Yu, D. Tsegaye Awugichew and X. Li, *Environ. Res.*, 2024, **257**, 119314.
41 X. Sun, X. Ni, X. Wang and D. Xu, *Surf. Interfaces*, 2022, **31**, 102053.
42 Y. Cheng, B. Wang, P. Yan, J. Shen, J. Kang, S. Zhao, X. Zhu, L. Shen, S. Wang, Y. Shen and Z. Chen, *Chem. Eng. J.*, 2023, **454**, 140232.
43 S. Mallikarjun Sharada, R. K. B. Karlsson, Y. Maimaiti, J. Voss and T. Bligaard, *Phys. Rev. B*, 2019, **100**, 035439.
44 S. Yang, X. Liu, S. He, C. Jia and H. Zhong, *J. Mol. Liq.*, 2024, **394**, 123688.
45 D. Zhang, Y. Liu, Y. Song, X. Sun, W. Liu, J. Duan and Z. Cai, *Sep. Purif. Technol.*, 2023, **313**, 123430.
46 V.-R. Le, T.-B. Nguyen, C.-W. Chen, C. P. Huang, X.-T. Bui and C.-D. Dong, *Sep. Purif. Technol.*, 2023, **315**, 123672.
47 Y. Yang, Y. Chi, K. Yang, Z. Zhang, P. Gu, X. Ren, X. Wang, H. Miao and X. Xu, *J. Colloid Interface Sci.*, 2023, **652**, 350–361.
48 M. Noman, G. Yu, E. A. Elimian and K. Yun, *J. Environ. Chem. Eng.*, 2025, **13**, 115236.
49 J. Zhang, L. Yang, C. Liu, J. Ma, C. Yan, S. Mu and M. Yu, *Sep. Purif. Technol.*, 2024, **340**, 126767.
50 J. Wang, Z. Huang, W. Liu, C. Chang, H. Tang, Z. Li, W. Chen, C. Jia, T. Yao, S. Wei, Y. Wu and Y. Li, *J. Am. Chem. Soc.*, 2017, **139**, 17281–17284.